

A BILEVEL LEARNING APPROACH FOR OPTIMAL OBSERVATION PLACEMENT IN VARIATIONAL DATA ASSIMILATION

P. CASTRO[†], J.C. DE LOS REYES[†]

ABSTRACT. In this paper we propose a bilevel optimization approach for the placement of observations in variational data assimilation problems. Within the framework of supervised learning, we consider a bilevel problem where the lower level task is the variational reconstruction of the initial condition of the system, and the upper level problem solves the optimal placement with help of a sparsity inducing norm. Due to the pointwise nature of the observations, an optimality system with regular Borel measures on the right-hand side is obtained as necessary and sufficient optimality condition for the lower level problem. The latter is then considered as constraint for the upper level instance, yielding an optimization problem constrained by time-dependent PDE's with measures. After proving some extra regularity results, we demonstrate the existence of Lagrange multipliers and derive a necessary optimality system characterizing the optimal solution of the bilevel problem. The numerical solution is carried out also on two levels. The lower level problem is solved using a standard BFGS method, while the upper level one is solved by means of a projected BFGS algorithm based on the estimation of ϵ -active sets. A penalty function is also considered for enhancing sparsity of the location weights. Finally some numerical experiments are presented to illustrate the main features of our approach.

1. INTRODUCTION

Data assimilation (DA) problems deal with the reconstruction of the initial condition of a dynamical system based on observations of the state, previous estimates and the system model, and are widely used in applications like, e.g., numerical weather prediction. These problems are important because the more accurate the initial condition, the better the quality of the forecast of the system state. There are several approaches to deal with data assimilation problems, such as, optimal interpolation, variational approaches or hybrid methods (see [15] and the references therein).

Variational approaches focus on solving an optimal least squares problem, and can be broadly classified in two classes, depending on the type of observations considered. The first one, three-dimensional variational analysis ($3D$ -VAR), considers observations in just one instant of time, while the second one, four-dimensional variational analysis ($4D$ -VAR), takes into account observations distributed in a given period of time $[t_0, t_n]$. The quality of the reconstruction strongly depends on the number of observations and their location in both space and time.

In several practical situations, the number of observations is scarce and it is important to optimally decide where to locate new devices/measurements. Several approaches have emerged in the last years in order to optimally place sensors in different settings. The most classical approach is the optimal filtering one, developed in the 70's to cope with Gaussian linear problems [3, 4, 8], and further developed in [5, 6, 13] to deal with nonlinear systems. An alternative observability approach for the location of sensors in linear parabolic and hyperbolic equations was recently developed in [19]. Additionally, in [1, 2] an A-optimal experimental design approach for the location of

sensors in systems governed by PDE's was developed, which was also applied to a thermo-mechanical data assimilation problem in [12].

In this paper we tackle the optimal placement problem using a bilevel learning approach [11, 10, 14]. In contrast to optimal experimental design strategies, our framework allows us to work with different quality measures, without making assumptions on the model statistics, and is not restricted to the A-, D- or E- optimal experimental design paradigms [20]. Moreover, differently from previous related contributions [11, 1, 2], we are able to analyze the resulting bilevel optimization problem in function spaces and get an insight into its complex mathematical structure. By considering measures in space and mollified Dirac measures in time, we are able to obtain well-posedness of the bilevel adjoint system and characterize minima by means of an optimality system.

The challenging numerical solution of the bilevel problem is carried out in two stages. For the upper level problem we use a projected BFGS method, whose inverse Hessian approximation is iteratively built upon the estimation of ϵ -active sets. For the lower level problem a standard BFGS algorithm is considered. To further enhance the sparsity of the solution vector, the linear penalization function is replaced by a concave one, with values between 0 and 1.

The proposed bilevel optimization framework for observation placement in the context of variational data assimilation problems, as well as the rigorous mathematical analysis of the upper- and lower-level problems constitute the genuine contribution of this manuscript. This is further complemented by the design of a second-order numerical algorithm for the solution of the problem, whose performance is computationally verified.

The structure of the paper is as follows. In Section 2 we study the variational data assimilation problem, and discuss existence and uniqueness of the solution to the adjoint equation with regular Borel measures on its right-hand side. Section 3 focuses on the existence of Lagrange multipliers and on the derivation of an optimality system for the bilevel optimal placement problem. In Section 4, we present a second-order solution algorithm for the problem and discuss convergence properties as well as numerical aspects. Finally, in the last section, several computational experiments are carried out to verify the main properties of the approach and the solution method.

2. VARIATIONAL DATA ASSIMILATION PROBLEM

In this paper, we focus on the 4D-VAR approach to solve the data assimilation problem, which may be expressed in general form as:

$$\begin{aligned}
 \min_u J(y, u) &= \frac{1}{2} \sum_{i=1}^l [H(y(t_i)) - z_o(t_i)]^T R_i^{-1} [H(y(t_i)) - z_o(t_i)] \\
 &\quad + \frac{1}{2} \int_{\Omega} (u - u^b) B^{-1} (u - u^b) dx \\
 \text{(1)} \quad & \\
 \text{subject to:} & \\
 y(t_i) &= M_i(y(t_0)) && \text{(system model),} \\
 y(t_0) &= u && \text{(initial condition),}
 \end{aligned}$$

where z_o represent the observed state, u^b the background information and H is the observation operator that transforms model variables into observable variables. For each $i = 1, \dots, l$, R_i represents the observation error covariance matrix at time t_i , and $B^{-1} \in \mathcal{L}(L^2(\Omega))$ is the background information error covariance positive operator.

Hereafter, we set for simplicity the observation error covariance matrices equal to the identity. We also introduce a weight matrix W , whose diagonal is a binary vector that represents a location vector $w = (w_k)$, $k = 1, \dots, n_s$, that takes the value one if the placement x_k is chosen and zero otherwise. Moreover, to be able to choose not only the optimal placements but also optimal time intervals, we consider a weight matrix for time as well. Its diagonal is a binary vector $\sigma = (\sigma_i)$, $i = 1, \dots, n_T$, which takes values one if the time subinterval i is chosen and zero if not.

As the dynamical system that represents the system model constraint, we consider an initial-value parabolic linear equation with homogeneous Dirichlet boundary conditions, $\partial_t y + Ay = 0$, where A is a linear elliptic second order differential operator

$$Ay(x) = - \sum_{i,j}^n D_i(a_{ij}(x)D_j y(x)), \quad \text{for } x \in \Omega,$$

with coefficients $(a_{ij}) \in L^\infty(\Omega, \mathbb{R}^{n \times n})$, for $i, j = 1, \dots, n$, satisfying the symmetry condition $a_{ij}(x) = a_{ji}(x)$ and the condition of uniform ellipticity, i.e., there exists a constant $\kappa > 0$ such that

$$\sum_{i,j}^n a_{ij} \xi_i \xi_j \geq \kappa |\xi|^2, \quad \forall \xi \in \mathbb{R}^n$$

for almost all $x \in \Omega$. Using the notation $a := (a_{ij})$, Green's identity is expressed as:

$$\int_{\Omega} g(x) A s(x) dx = - \int_{\Gamma} g(x) \partial_{\nu_A} s(x) dx + \int_{\Omega} a \nabla g(x) \cdot \nabla s(x) dx.$$

where ∂_{ν_A} denotes the directional derivative in the direction of the conormal vector ν_A ([21, p.37]).

The variational data assimilation problem we will study consists in the following: Find $u \in L^2(\Omega)$ solution of

$$(2) \quad \min_u J(y, u) = \frac{1}{2} \int_0^T \sum_{k,i} w_k \sigma_i \rho_i(t) [y(x_k, t) - z_o(x_k, t)]^2 dt + \frac{1}{2} \|u - u_b\|_{B^{-1}}^2 + \frac{\vartheta}{2} \|\nabla(u - u_b)\|_{L^2(\Omega)}^2$$

$$(3) \quad \text{subject to: } \begin{cases} \frac{\partial y}{\partial t} + Ay = 0 & \text{in } Q = \Omega \times]0, T[\\ y = 0 & \text{on } \Sigma = \Gamma \times]0, T[\\ y(x, 0) = u & \text{in } \Omega. \end{cases}$$

where $\|u - u_b\|_{B^{-1}}^2 := \int_{\Omega} (u - u_b) B^{-1} (u - u_b) dx$ and $\vartheta > 0$ is a regularization parameter, which in practice can be as small as required. In (2), we also consider regular support functions $\rho_i(t) \in C^2(0, T)$, for each $i = 1, \dots, n_T$, that act as mollifiers and let us consider short time-interval observations (almost instantaneous). The purpose of adding this kind of functions is to consider mollified Dirac measures in time in the analysis of the variational data assimilation problem.

2.1. Existence of a solution for the DA problem. Let $\Omega \subset \mathbb{R}^n$, $1 < n \leq 3$, be a bounded domain of class \mathcal{C}^2 , $Q := \Omega \times (0, T)$ and $\Sigma := \Gamma \times (0, T)$, with $T > 0$ a fixed real number. The constraint of the data assimilation problem, given by (3), is a linear problem which is well-posed in the following sense: For each $u = u(x) \in L^2(\Omega)$, there exists a unique weak solution $y = y(x, t) \in W(0, T)$ such that

$$(4) \quad - \int_0^T \int_{\Omega} y v_t dx dt + \int_0^T \int_{\Omega} a \nabla y \cdot \nabla v dx dt = \int_{\Omega} u v(0) dx - \int_{\Omega} y(T) v(T) dx, \forall v \in W(0, T),$$

where $W(0, T)$ is the Hilbert space of functions in $L^2(0, T; H_0^1(\Omega))$ with time partial derivative in $L^2(0, T; H^{-1}(\Omega))$.

Since the coefficients of A and the right-hand side of the linear equation are sufficiently regular, we can get extra regularity results. In fact, if $u \in H^1(\Omega)$, there exists a unique solution $y \in H^{2,1}(Q)$ of (3), where

$$H^{2,1}(Q) = \left\{ g, \frac{\partial g}{\partial x_i}, \frac{\partial^2 g}{\partial x_i \partial x_j}, \frac{\partial g}{\partial t} \in L^2(Q) \right\}$$

is a Hilbert space. Moreover, the following estimate between $u \in H^1(\Omega)$ and $y \in H^{2,1}(Q)$ is also verified (see [17], pp.341)

$$(5) \quad \|y\|_{H^{2,1}(Q)} \leq c \|u\|_{H^1(\Omega)}, \text{ for some constant } c > 0.$$

Therefore, the solution mapping that assigns $H^1(\Omega) \ni u \mapsto y(u) \in H^{2,1}(Q)$ is a linear and continuous isomorphism. Rewriting the objective functional in (2) by taking into account the solution mapping $y(u)$, we get the reduced optimization problem:

$$(6) \quad \min_u f(u) = \frac{1}{2} \int_0^T \int_{\Omega} \sum_{k,i} w_k \sigma_i \rho_i(t) [y(u)(x, t) - z_o(x, t)]^2 \delta(x - x_k) dt dx \\ + \frac{1}{2} \|u - u_b\|_{B^{-1}}^2 + \frac{\vartheta}{2} \|\nabla(u - u_b)\|_{L^2}^2.$$

Notice that f is convex since w_k , σ_i and $\rho_i(t)$ are positive for every $i \in \{1, \dots, n_T\}$ and every $k \in \{1, \dots, n_s\}$. Hence, f can be seen as a conical combination of convex functions. In the same way, f is a continuous functional since the solution operator and the norm are. Therefore, f is weakly lower semicontinuous and, moreover,

$$(7) \quad f(u) \geq \frac{1}{2} \|u - u_b\|_{B^{-1}}^2 + \frac{\vartheta}{2} \|\nabla(u - u_b)\|_{L^2(\Omega)}^2 \geq c_B \|u - u_b\|_{H^1(\Omega)}^2, \quad c_B > 0$$

where $u_b \in H^1(\Omega)$ is known, and corresponds to the background information. Note that thanks to the embedding $H^{2,1}(Q) \hookrightarrow L^2(0, T; C(\bar{\Omega}))$ (see [7, p.31]), the continuity of the state in the spatial variable holds, and the pointwise evaluations of $y(u)$ in the space component are well defined.

Theorem 1. *Problem (6) has a unique optimal solution $\bar{u} \in H^1(\Omega)$ with $\bar{y} = y(\bar{u}) \in H^{2,1}(Q)$ its related optimal state.*

Proof. Let $\{u_n\}_{n \geq 1} \subset H^1(\Omega)$ be a minimizing sequence, i.e.,

$$\inf_{u \in H^1(\Omega)} f(u) = \lim_{n \rightarrow +\infty} f(u_n).$$

From (7), f is radially unbounded and, therefore, the sequence $\{u_n\}$ is bounded in $H^1(\Omega)$. Since $H^1(\Omega)$ is a reflexive space, there exists a weakly convergent subsequence $\{u_{n_k}\} \subset \{u_n\}$ and a limit point $\bar{u} \in H^1(\Omega)$ such that $u_{n_k} \rightharpoonup \bar{u}$ as $k \rightarrow \infty$. Due to the continuity of the solution operator and the weakly lower semi continuity of f , we then get that

$$f(\bar{u}) \leq \liminf_{k \rightarrow \infty} f(u_{n_k}) = \inf_{u \in H^1(\Omega)} f(u).$$

Consequently, $\bar{u} \in H^1(\Omega)$ is an optimal solution of (6). The uniqueness of the solution follows from the strict convexity of f . \square

2.2. Adjoint equation. As a preparatory step for the derivation of an optimality system for the variational data assimilation problem, we consider the following problem:

$$(8) \quad \begin{aligned} -p_t + Ap &= \mu & \text{in } Q \\ p &= 0 & \text{on } \Sigma \\ p(x, T) &= 0 & \text{in } \Omega, \end{aligned}$$

with $\mu \in L^2(0, T; \mathcal{M}(\Omega))$. Here, $\mathcal{M}(\Omega)$ represents the space of regular Borel measures in Ω and $L^2(0, T; \mathcal{M}(\Omega))$ the space of weakly measurable functions. It is important to remark that considering the right-hand side of (8) in $\mathcal{M}(Q)$ leads to an ill-posed problem ([7, p.29]).

Definition 1. We call $p \in L^2(Q)$ a very weak solution to (8) if the following is verified:

$$(9) \quad \int_0^T \int_{\Omega} p(\varphi_t + A\varphi) dx dt = \int_0^T \langle \mu(t), \varphi(t) \rangle_{\mathcal{M}(\Omega), C(\bar{\Omega})} dt - \int_{\Omega} p(0)\varphi(0) dx, \quad \forall \varphi \in \Psi,$$

where $\Psi = \{\varphi \in H^{2,1}(Q) : \varphi = 0 \text{ on } \Sigma\}$.

In the theorem below, we show existence of a unique solution for equation (8).

Theorem 2. Problem (8) has a unique very weak solution $p \in L^2(Q)$. Moreover, if $\mu \in L^2(0, T; \mathcal{M}(\Omega))$, p belongs to $L^2(0, T; W_0^{1,r}(\Omega))$ for every $r \in [1, \frac{n}{n-1}[$, and there exists a constant $c_p > 0$ such that

$$(10) \quad \|p\|_{L^2(0,T;W_0^{1,r}(\Omega))} \leq c_p \|\mu\|_{L^2(0,T;\mathcal{M}(\Omega))}.$$

Proof. First, we will prove the existence of a unique very weak solution $p \in L^2(Q)$ to equation (8). Let us introduce the following auxiliary problem: For a given function $\phi \in L^2(Q)$, find φ solution of

$$(11) \quad \begin{aligned} \varphi_t + A\varphi &= \phi & \text{in } Q \\ \varphi &= 0 & \text{on } \Sigma \\ \varphi(x, 0) &= 0 & \text{in } \Omega. \end{aligned}$$

Equation (11) has a unique solution $\varphi \in \Psi$ ([18], pp.182). Therefore, the operator $\partial_t + A : \Psi \mapsto L^2(Q)$ defines a bijective isomorphism.

Multiplying the auxiliary problem by $p \in L^2(Q)$, we get

$$(12) \quad \langle \varphi_t + A\varphi, p \rangle_{L^2(Q), L^2(Q)} = \langle \phi, p \rangle_{L^2(Q), L^2(Q)}.$$

By transposition of the isomorphism $\Psi \ni \varphi \mapsto \varphi_t + A\varphi = \phi \in L^2(Q)$, we get the existence of a unique $p \in L^2(Q)$ very weak solution of (9), with $\mu \in \Psi^*$.

Assuming that the right-hand side of the equation belongs to $L^2(0, T; \mathcal{M}(\Omega))$ and using [7, Theorem 2.2], we additionally get that $p \in L^2(0, T; W_0^{1,r}(\Omega))$ with $r \in [1, \frac{n}{n-1}[$ and estimate (10) is verified. \square

Remark 1. The continuity of the solution of (8) in the time variable is also verified. Specifically, $p \in C(0, T; L^2(\Omega))$ (see [7, Remark 2.3, p.32]).

2.3. Optimality system. In this section we state the first order optimality conditions satisfied by the solution $\bar{u} \in H^1(\Omega)$ of the variational data assimilation problem given by (6) and $\bar{y} = y(\bar{u}) \in H^{2,1}(Q)$ its related optimal state.

Theorem 3. *Let $\bar{u} \in H^1(\Omega)$ be a solution to (6) with $\bar{y} \in H^{2,1}(Q)$ its associated optimal state. Then, there exists a unique adjoint state $\bar{p} \in L^2(0, T; W^{1,r}(\Omega))$, with $r \in \left[1, \frac{n}{n-1}\right]$ satisfying:*

State equation (in strong form):

$$(13a) \quad \begin{aligned} \bar{y}_t + A\bar{y} &= 0 & \text{in } Q = \Omega \times]0, T[\\ \bar{y} &= 0 & \text{on } \Sigma = \Gamma \times]0, T[\\ \bar{y}(x, 0) &= \bar{u} & \text{in } \Omega. \end{aligned}$$

Adjoint equation (in very weak form):

$$(13b) \quad \begin{aligned} -\bar{p}_t + A\bar{p} &= \sum_{k,i} w_k \sigma_i \rho_i(t) [\bar{y}(x, t) - z_o(x, t)] \otimes \delta(x - x_k) & \text{in } Q \\ \bar{p} &= 0 & \text{on } \Sigma \\ \bar{p}(x, T) &= 0 & \text{in } \Omega. \end{aligned}$$

Gradient equation (in weak form):

$$(13c) \quad \begin{aligned} -\vartheta \Delta(\bar{u} - u_b) + B^{-1}(\bar{u} - u_b) + \bar{p}(0) &= 0 & \text{in } \Omega \\ \partial_\nu(\bar{u} - u_b) &= 0 & \text{on } \Gamma. \end{aligned}$$

Proof. We start by computing the derivative of the reduced cost functional (6) at $\bar{u} \in H^1(\Omega)$

$$\begin{aligned} f'(\bar{u})h &= \int_{\Omega} \int_0^T \sum_{k,i} w_k \sigma_i \rho_i(t) [y(\bar{u})(x_k, t) - z_o(x_k, t)] \delta(x - x_k) y'(\bar{u}) dx dt \\ &\quad + \int_{\Omega} (\bar{u}(x) - u_b(x)) B^{-1} h dx + \vartheta \int_{\Omega} \nabla(\bar{u} - u_b) \cdot \nabla h dx, \quad \forall h \in H^1(\Omega), \end{aligned}$$

where $y'(\bar{u}) \in \Psi$ is the unique strong solution to the linearized equation:

$$\begin{aligned} \frac{\partial y'(\bar{u})}{\partial t} + Ay'(\bar{u}) &= 0 & \text{in } Q \\ y'(\bar{u}) &= 0 & \text{on } \Sigma \\ y'(\bar{u})(x, 0) &= h & \text{in } \Omega. \end{aligned}$$

On the other hand, setting $s(x, t) = \bar{y}(x, t) - z_o(x, t)$ and $\delta_k = s(x, \cdot) \otimes \delta(x - x_k)$ with $\delta(x - x_k) \in \mathcal{M}(\Omega)$ for each $k \in \{1, \dots, n_S\}$, we have that $\delta_k \in L^2(0, T; \mathcal{M}(\Omega))$.

In fact,

$$\begin{aligned}
\|s(x, \cdot) \otimes \delta(x - x_k)\|_{L^2(0,T;\mathcal{M}(\Omega))} &= \int_0^T \|s(x, t) \otimes \delta(x - x_k)\|_{\mathcal{M}(\Omega)}^2 dt \\
&= \int_0^T \left(\sup_{\Omega} \left\{ \int g(x) s(x, t) \delta(x - x_k) dx : g \in C_0(\bar{\Omega}) \text{ and } \|g\|_{\infty} \leq 1 \right\} \right)^2 dt \\
&= \int_0^T \left(\sup_{\|g\|_{\infty} \leq 1} \{g(x_k) s(x_k, t)\} \right)^2 dt \leq \int_0^T \left(s(x_k, t) \sup_{\|g\|_{\infty} \leq 1} \{|g(x_k)|\} \right)^2 dt \\
&= \int_0^T |s(x_k, t)|^2 dt < +\infty.
\end{aligned}$$

The result follows since for each $k \in \{1, \dots, n_S\}$ and $i \in \{1, \dots, n_T\}$, w_k , σ_i , and $\rho_i(t)$ are positive values and the sums involved are finite. Hence, there exists $\bar{p} \in L^2(Q)$ unique solution of the adjoint equation

$$\begin{aligned}
(14) \quad \int_{\Omega} \int_0^T (\varphi_t - A\varphi) \bar{p} dx dt + \int_{\Omega} \varphi(0) \bar{p}(0) dx \\
= \int_0^T \sum_{k,i} w_k \sigma_i \rho_i(t) [y(\bar{u})(x_k, t) - z_o(x_k, t)] \varphi(x_k, t) dt, \quad \forall \varphi \in \Psi.
\end{aligned}$$

Additionally, using Theorem 2, we can conclude that $\bar{p} \in L^2(0, T; W^{1,r}(\Omega))$, with $r \in [1, \frac{n}{n-1}[$.

Using the adjoint equation (13b), tested with $y'(\bar{u}) \in \Psi$, it follows that

$$\begin{aligned}
f'(\bar{u})h &= \int_{\Omega} \int_0^T \bar{p} \left(\frac{\partial y'(\bar{u})}{\partial t} + Ay'(\bar{u}) \right) dx dt + \int_{\Omega} \bar{p}(0) h dx \\
&\quad + \int_{\Omega} (\bar{u}(x) - u_b(x)) B^{-1} h dx + \vartheta \int_{\Omega} \nabla(\bar{u} - u_b) \cdot \nabla h dx = 0, \quad \forall h \in H^1(\Omega).
\end{aligned}$$

Considering the linearized equation in the above inequality, we get

$$(15) \quad \int_{\Omega} (\bar{u}(x) - u_b(x)) B^{-1} h dx + \vartheta \int_{\Omega} \nabla(\bar{u} - u_b) \cdot \nabla h dx + \int_{\Omega} \bar{p}(0) h dx = 0, \quad \forall h \in H^1(\Omega),$$

which correspond to the weak form of (13c). \square

Corollary 1. *The adjoint state $\bar{p} \in L^2(0, T; W_0^{1,r}(\Omega))$ for every $r \in [1, \frac{n}{n-1}[$ verifies the following estimate*

$$(16) \quad \|\bar{p}\|_{L^2(0,T;W_0^{1,r}(\Omega))} \leq \hat{c}(\|w\|_{\mathbb{R}^{n_S}} + \|\sigma\|_{\mathbb{R}^{n_T}}), \quad \hat{c} > 0.$$

Proof. Using the estimate in Theorem 2 into the adjoint equation, we get

$$(17) \quad \|\bar{p}\|_{L^2(0,T;W_0^{1,r}(\Omega))} \leq c_p \sum_{k,i} \|w_k \sigma_i \rho_i(t) \delta_k\|_{L^2(0,T;\mathcal{M}(\Omega))}.$$

Applying Young's inequality to the above estimate, we have

$$\begin{aligned}
\|p\|_{L^2(0,T;W_0^{1,r}(\Omega))} &\leq c_p \sum_{k,i} \left\| \left(\frac{w_k^2}{2} + \frac{\sigma_i^2}{2} \right) \rho_i(t) \delta_k \right\|_{L^2(0,T;\mathcal{M}(\Omega))} \\
&\leq c_p \left(\sum_{k,i} \left\| \frac{w_k^2}{2} \rho_i(t) \delta_k \right\|_{L^2(0,T;\mathcal{M}(\Omega))} + \sum_{k,i} \left\| \frac{\sigma_i^2}{2} \rho_i(t) \delta_k \right\|_{L^2(0,T;\mathcal{M}(\Omega))} \right) \\
&\leq c_p \left(\frac{1}{2} \max_k \{w_k^2\} \sum_{k,i} \|\rho_i(t) \delta_k\|_{L^2(0,T;\mathcal{M}(\Omega))} + \frac{1}{2} \max_i \{\sigma_i^2\} \sum_{k,i} \|\rho_i(t) \delta_k\|_{L^2(0,T;\mathcal{M}(\Omega))} \right) \\
&\leq c_p \left(\frac{1}{2} \max_k \{w_k\} + \frac{1}{2} \max_i \{\sigma_i\} \right) \sum_{k,i} \|\rho_i(t) \delta_k(t)\|_{L^2(0,T;\mathcal{M}(\Omega))}^2 dt \leq \hat{c} (\|w\|_\infty + \|\sigma\|_\infty).
\end{aligned}$$

The last inequality follows taking $\hat{c} = \frac{c_p}{2} n_s n_T$ and since $\|\rho_i(t) \delta_k(t)\|_{L^2(0,T;\mathcal{M}(\Omega))} \leq 1$. In fact,

$$\begin{aligned}
\|\rho_i(t) \delta_k(t)\|_{L^2(0,T;\mathcal{M}(\Omega))} &= \int_0^T \left(\sup \left\{ \int_\Omega f(x,t) \otimes \rho_i(t) \delta(x-x_k) dx : \|f\|_\infty \leq 1 \right\} \right)^2 dt \\
&\leq \int_0^T \left(\rho_i(t) \sup_{\|f\|_\infty \leq 1} |f(x_k,t)| \right)^2 dt \leq \int_0^T \rho_i(t)^2 dt \leq 1.
\end{aligned}$$

Thanks to the norm equivalence in \mathbb{R}^N and the inequalities above, the result holds. \square

3. BILEVEL OPTIMAL PLACEMENT PROBLEM

Depending on the amount of observations, data assimilation methods may be more or less efficient in reconstructing a useful initial condition. In meteorology, for instance, data may be collected through meteorological stations, satellite images, radiosondes, among others. In practice, the installation and operational costs of such observation devices may be too high and it is important to locate them in an optimal way, meaning that as few as possible should be placed and the richest amount of information should be measured, to accomplish a desired goal. To pose these types of placement problems in a mathematical (and solvable) way has been a challenge for the last 50 years [3, 4, 8, 5, 6, 13, 19, 1, 2, 12].

In this paper our goal actually consists in determining where new observation devices should be placed and when the measurements should be taken, to get new valuable information for the data assimilation process and, as a consequence, a better reconstruction of the initial condition. We tackle the aforementioned problem by considering a supervised learning approach in which we presuppose the existence of a training set $\left\{ \left(u_1^\dagger, y_1^\dagger \right), \dots, \left(u_N^\dagger, y_N^\dagger \right) \right\}$, consisting of improved (with exceptionally more observations) reconstructions of the initial conditions and the corresponding simulations of the system state. The idea of working with training sets is borrowed from machine learning and is a widespread practice nowadays. In our case, the information that we want to learn is precisely the vector of optimal placements w and optimal time intervals σ at which the measurements should be carried out.

3.1. Problem statement. To accomplish the mentioned goal, we consider a bilevel optimization approach where the lower level is related to finding a solution to the variational data assimilation problem, while the upper level solves the optimal placement

In the next theorem existence of a unique solution to system (19b), for each $w \in \mathbb{R}^{n_s}$ and $\sigma \in \mathbb{R}^{n_T}$, is verified.

Theorem 4. *For each $w \in \mathbb{R}^{n_s}$ and $\sigma \in \mathbb{R}^{n_T}$, the state system (19b) has a unique solution*

$$\mathbf{y}_j = (y_j, p_j, u_j) \in H^{2,1}(Q) \times X \times H^1(\Omega) =: \mathbf{Y}, \quad j \in 1, \dots, N,$$

where $X = L^2(0, T; W^{1,r}(\Omega))$ with $r \in [1, \frac{n}{n-1}[$. Moreover, the following estimate holds:

$$\|\mathbf{y}\|_{\mathbf{Y}^N} \leq C(\|w\|_{\mathbb{R}^{n_s}} + \|\sigma\|_{\mathbb{R}^{n_T}}), \quad \text{for some } C > 0.$$

Proof. The state system corresponds to N optimality systems of the data assimilation problem given by (13a)-(13c). Existence and uniqueness of $y_j \in H^{2,1}(Q)$ solution of (13a), $p_j \in X$ solution of (13b) and the gradient equation (13c) was previously verified for each $u_j \in H^1(\Omega)$, $j \in 1, \dots, N$. To prove the estimate, notice that

$$\|\mathbf{y}_j\|_{\mathbf{Y}} = \|(y_j(\mathbf{w}), p_j(\mathbf{w}), u_j(\mathbf{w}))\|_{\mathbf{Y}} = \|y_j(\mathbf{w})\|_{H^{2,1}(Q)} + \|p_j(\mathbf{w})\|_X + \|u_j(\mathbf{w})\|_{H^1(\Omega)}.$$

From (16) the following estimate holds: $\|p_j(\mathbf{w})\|_X \leq c_{pj}(\|w\|_{\mathbb{R}^{n_s}} + \|\sigma\|_{\mathbb{R}^{n_T}})$. Moreover, using the weak formulation of the gradient equation and testing with $h = (u - u_b) \in H^1(\Omega)$ we get

$$\|u - u_b\|_{B^{-1}}^2 + \vartheta \|\nabla(u - u_b)\|_{L^2(\Omega)}^2 \leq |\langle p(0), u - u_b \rangle_{H^{-1}, H^1}| \leq \|p(0)\|_{H^{-1}} \|u - u_b\|_{H^1}.$$

Since the first norm is equivalent to the L^2 -norm and applying the reverse triangle inequality and the Archimedian property, we get an estimate for the control variable

$$\|u\|_{H^1} \leq \|p(0)\|_{H^{-1}} + \|u_b\|_{H^1} \leq (1 + z)\|p(0)\|_{H^{-1}}, \quad z \in \mathbb{N}$$

Using the estimate given by (5) and the inequality above, it follows that

$$\|y_j(\mathbf{w})\|_{H^{2,1}} \leq c\|u_j(\mathbf{w})\|_{H^1} \leq c_{yj}(\|w\|_{\mathbb{R}^{n_s}} + \|\sigma\|_{\mathbb{R}^{n_T}}).$$

Thus,

$$(20) \quad \|\mathbf{y}_j\|_{\mathbf{Y}} \leq (c_{yj} + c_{pj} + c_{uj})(\|w\|_{\mathbb{R}^{n_s}} + \|\sigma\|_{\mathbb{R}^{n_T}}) := c_j(\|w\|_{\mathbb{R}^{n_s}} + \|\sigma\|_{\mathbb{R}^{n_T}})$$

and the result follows. \square

3.2. Existence of solution for the bilevel optimization problem. The results of Theorem 4 imply the continuity and linearity of the solution mapping that assigns each $\mathbf{w} \in \mathbb{R}^{n_s} \times \mathbb{R}^{n_T}$ to its corresponding $\mathbf{y}(\mathbf{w}) \in \mathbf{Y}^N$. The variable \mathbf{y} can be written as $\mathbf{y}(\mathbf{w}) = (y(\mathbf{w}), p(\mathbf{w}), u(\mathbf{w}))$, if its components are rearranged, with $y = (y_1, \dots, y_N)$, $p = (p_1, \dots, p_N)$ and $u = (u_1, \dots, u_N)$. Therefore, the solution mapping S is given by

$$\mathbb{R}^{n_s} \times \mathbb{R}^{n_T} \ni \mathbf{w} \rightarrow S\mathbf{w} = (S_1(\mathbf{w}), S_2(\mathbf{w}), S_3(\mathbf{w})) = (y, p, u) \in \mathbf{Y}^N.$$

Rewriting the objective functional using the operator S , we obtain the following reduced functional

$$(21) \quad \min_{0 \leq \mathbf{w} \leq 1} F(\mathbf{w}) = \sum_{j=1}^N \|y_j^\dagger - (S_1(\mathbf{w}))_j\|^2 + \beta \sum_{j=1}^N \|u_j^\dagger - (S_3(\mathbf{w}))_j\|^2 + \gamma \sum_k w_k + \gamma \sigma \sum_i \sigma_i.$$

Let us remark that $F : \mathbb{R}^{n_s} \times \mathbb{R}^{n_T} \rightarrow \mathbb{R}$ given by (21) is strictly convex and continuous, so that it is weakly lower semicontinuous.

Theorem 5. *The minimization problem (21) has a unique optimal solution given by $\bar{\mathbf{w}} = (\bar{w}, \bar{\sigma}) \in \mathbb{R}^{n_s} \times \mathbb{R}^{n_T}$ with $\bar{\mathbf{y}} = \mathbf{y}(\bar{\mathbf{w}}) \in \mathbf{Y}^N$ its corresponding optimal state.*

Proof. Let us introduce the admissible set of placements

$$V_{ad} = \{\mathbf{w} = (w, \sigma) \in \mathbb{R}^{n_s} \times \mathbb{R}^{n_T} : 0 \leq w \leq 1, 0 \leq \sigma \leq 1\}$$

Since $F(\mathbf{w}) \geq 0$, there exists an infimum value, $j := \inf_{\mathbf{w} \in V_{ad}} F(\mathbf{w})$, and there is a sequence $\{\mathbf{w}_n\}_{n \geq 1} \subset V_{ad}$ such that

$$\lim_{n \rightarrow \infty} F(\mathbf{w}_n) = \inf_{\mathbf{w} \in V_{ad}} F(\mathbf{w}).$$

On the other hand as $V_{ad} \subset \mathbb{R}^{n_s} \times \mathbb{R}^{n_T}$ belongs to a finite dimensional space, and it is bounded, closed, and convex, V_{ad} is sequentially compact ([21], pp.47). Consequently, there exists a subsequence $\{\mathbf{w}_{n_k}\} \subset \{\mathbf{w}_n\}$ which converges to some $\bar{\mathbf{w}} \in V_{ad}$, i.e., $\mathbf{w}_{n_k} \rightarrow \bar{\mathbf{w}}$. Since S is linear and continuous, and F is w.l.s.c, we have

$$F(\bar{\mathbf{w}}) \leq \liminf_{k \rightarrow \infty} F(\mathbf{w}_{n_k}) = \inf_{\mathbf{w} \in V_{ad}} F(\mathbf{w}).$$

Therefore $\bar{\mathbf{w}} \in V_{ad}$ is an optimal solution of (21). The uniqueness of the solution follows from the strict convexity of F . \square

3.3. Optimality System. To formally derive the optimality system for the bilevel placement problem, we will use the Lagrangian approach. For each $j = 1, \dots, N$, we consider the optimality system of the lower-level data assimilation problem, given by:

$$(22a) \quad \begin{aligned} \frac{\partial y_j}{\partial t} + Ay_j &= 0 && \text{in } L^2(Q), \\ y_j &= 0 && \text{on } \Gamma, \\ y_j(0) &= u_j, && \text{in } \Omega \end{aligned}$$

$$(22b) \quad \int_{\Omega} \int_0^T \left(\frac{\partial \zeta_j}{\partial t} - A\zeta_j \right) p_j dx dt + \int_{\Omega} p_j(0) \zeta_j(0) dx \\ - \int_{\Omega} \int_0^T \zeta_j \left(\sum_{k,i} w_k \sigma_i \rho_i(t) [y_j(x, t) - z_{oj}(x, t)] \delta(x - x_k) \right) dx dt = 0, \forall \zeta_j \in \Psi,$$

$$(22c) \quad \int_{\Omega} (u_j(x) - u_{bj}(x)) B^{-1} \tau_j dx + \vartheta \int_{\Omega} \nabla(u_j - u_{bj}) \cdot \nabla \tau_j dx \\ + \int_{\Omega} p_j(0) \tau_j dx = 0, \forall \tau_j \in H^1(\Omega).$$

Formulations (22b) and (22c) represent the very weak and the weak forms of the adjoint and the gradient equation, respectively. Setting $\varrho = (\varrho_1, \dots, \varrho_N)$ as the Lagrangian multiplier, where $\varrho_j = (\eta_j, \varphi_j, \zeta_j, \tau_j) \in L^2(Q) \times (H^1(\Omega))^* \times \Psi \times H^1(\Omega)$ for each $j =$

$1, \dots, N$, the Lagrangian is given by

$$\begin{aligned} \mathcal{L}(\mathbf{y}, \mathbf{w}, \varrho) = & J(\mathbf{y}, \mathbf{w}) + \sum_{j=1}^N \left[\int_0^T \int_{\Omega} \eta_j \left(\frac{\partial y_j}{\partial t} + A y_j \right) dx dt + \int_{\Omega} \varphi_j (y_j(0) - u_j) dx \right. \\ & + \int_0^T \int_{\Omega} \left(\frac{\partial \zeta_j}{\partial t} + A \zeta_j \right) p_j dx dt + \int_{\Omega} p_j(0) \zeta_j(0) dx \\ & - \int_0^T \int_{\Omega} \zeta_j \left(\sum_{k,i} w_k \sigma_i \rho_i(t) [y_j(x, t) - z_{oj}(x, t)] \delta(x - x_k) \right) dx dt \\ & \left. + \int_{\Omega} (u_j(x) - u_{bj}(x)) B^{-1} \tau_j dx + \vartheta \int_{\Omega} \nabla(u_j - u_{bj}) \cdot \nabla \tau_j dx + \int_{\Omega} p_j(0) \tau_j dx \right] \end{aligned}$$

The bilevel adjoint system is obtained by setting the derivative of $\mathcal{L}(\mathbf{y}, \mathbf{w}, \varrho)$ with respect to \mathbf{y} , in a direction v , equal to zero, i.e., $\mathcal{L}_{\mathbf{y}_j}(v_j) = 0$, for all $j = 1, \dots, N$. First, taking the derivative with respect to y_j , in direction v_1^j , we obtain

$$\begin{aligned} \mathcal{L}_{y_j}(v_1^j) = & - \int_{\Omega} \int_0^T 2(y_j^\dagger - y_j) v_1^j dx dt + \int_{\Omega} \int_0^T \eta_j \left(\frac{\partial v_1^j}{\partial t} + A v_1^j \right) dx dt \\ & + \int_{\Omega} \varphi_j(0) v_1^j(0) dx - \int_{\Omega} \int_0^T \left(\sum_{k,i} w_k \sigma_i \rho_i(t) \zeta_j(x, t) \delta(x - x_k) \right) v_1^j dx dt = 0. \end{aligned}$$

which implies that η_j solves, in a very weak sense, the following PDE:

$$(23) \quad \begin{aligned} -\frac{\partial \eta_j}{\partial t} + A \eta_j &= 2(y_j^\dagger - y_j) + \sum_{k,i} w_k \sigma_i \rho_i(t) \zeta_j(x, t) \otimes \delta(x - x_k) && \text{in } \Omega \times]0, T[\\ \eta_j &= 0 && \text{on } \Gamma \times]0, T[\\ \eta_j(T) &= 0 && \text{in } \Omega, \end{aligned}$$

and, additionally, $\varphi_j = \eta_j(0)$. Now, taking the derivative with respect to p_j , in direction v_2^j , we get

$$\mathcal{L}_{p_j}(v_2^j) = \int_{\Omega} \int_0^T \left(\frac{\partial \zeta_j}{\partial t} + A \zeta_j \right) v_2^j dx dt + \int_{\Omega} v_2^j(0) (\zeta_j(0) + \tau_j) dx = 0$$

and, consequently, ζ_j is strong solution of

$$(24) \quad \begin{aligned} \frac{\partial \zeta_j}{\partial t} + A \zeta_j &= 0 && \text{in } \Omega \times]0, T[\\ \zeta_j &= 0 && \text{on } \Gamma \times]0, T[\\ \zeta_j(0) &= -\tau_j && \text{in } \Omega. \end{aligned}$$

Finally, taking the derivative with respect to u_j , in direction v_3^j ,

$$\mathcal{L}_{u_j}(v_3^j) = \int_{\Omega} - \left(2\beta(u_j^\dagger - u_j) + \varphi_j \right) v_3^j dx + \int_{\Omega} v_3^j B^{-1} \tau_j dx + \vartheta \int_{\Omega} \nabla v_3^j \cdot \nabla \tau_j dx = 0,$$

and, consequently, τ_j is the unique weak solution of

$$(25) \quad \begin{aligned} -\vartheta \Delta \tau_j + B^{-1} \tau_j &= 2\beta(u_j^\dagger - u_j) + \varphi_j && \text{in } \Omega \\ \partial_\nu \tau_j &= 0 && \text{on } \Gamma. \end{aligned}$$

Theorem 6. *Let $(\bar{w}, \bar{\sigma}) \in \mathbb{R}^{n_s} \times \mathbb{R}^{n_T}$ be an optimal solution to (19) with $\bar{\mathbf{y}} = \mathbf{y}(\bar{\mathbf{w}}) \in \mathbf{Y}^N$ its corresponding optimal state. Then, there exists a unique adjoint state $(\eta_j, \zeta_j, \tau_j) \in X \times H^{2,1}(Q) \times H^1(\Omega)$, for all $j = 1, \dots, N$, and Karush-Kuhn-Tucker multipliers $\lambda^a, \lambda^b \in \mathbb{R}^{n_s} \times \mathbb{R}^{n_T}$ satisfying:*

Adjoint system: For all $j = 1, \dots, N$,

$$(26a) \quad \begin{aligned} -\frac{\partial \eta_j}{\partial t} + A \eta_j &= 2(y_j^\dagger - y_j) + \sum_{k,i} w_k \sigma_i \rho_i(t) \zeta_j(x, t) \otimes \delta(x - x_k) && \text{in } \Omega \times]0, T[\\ \eta_j &= 0 && \text{on } \Gamma \times]0, T[\\ \eta_j(T) &= 0 && \text{in } \Omega \end{aligned}$$

$$(26b) \quad \begin{aligned} \frac{\partial \zeta_j}{\partial t} + A \zeta_j &= 0 && \text{in } \Omega \times]0, T[\\ \zeta_j &= 0 && \text{on } \Gamma \times]0, T[\\ \zeta_j(0) &= -\tau_j && \text{in } \Omega \end{aligned}$$

$$(26c) \quad \begin{aligned} -\vartheta \Delta \tau_j + B^{-1} \tau_j &= 2\beta(u_j^\dagger - u_j) + \eta_j(0) && \text{in } \Omega \\ \partial_\nu \tau_j &= 0 && \text{on } \Gamma, \end{aligned}$$

very weakly, strongly and weakly, respectively,

Gradient system:

$$(26d) \quad \begin{aligned} \gamma_w - \sum_{j=1}^N \int_0^T \sum_i \sigma_i \rho_i(t) \zeta_j(x_k, t) (y_j(x_k, t) - z_{oj}(x_k, t)) dt \\ = \lambda_k^a - \lambda_k^b, \quad \text{for all } k = 1, \dots, n_s, \end{aligned}$$

$$(26e) \quad \begin{aligned} \gamma_\sigma - \sum_{j=1}^N \int_0^T \sum_k w_k \rho_i(t) \zeta_j(x_k, t) (y_j(x_k, t) - z_{oj}(x_k, t)) dt \\ = \lambda_{n_s+i}^a - \lambda_{n_s+i}^b, \quad \text{for all } i = 1, \dots, n_T, \end{aligned}$$

Complementarity system:

$$(26f) \quad \begin{aligned} \lambda_\ell^a \geq 0, \lambda_\ell^b \geq 0, &&& \text{for all } \ell = 1, \dots, n_s + n_T \\ \lambda_k^a \bar{w}_k = \lambda_k^b (\bar{w}_k - 1) = 0, &&& \text{for all } k = 1, \dots, n_s \\ \lambda_{n_s+i}^a \bar{\sigma}_i = \lambda_{n_s+i}^b (\bar{\sigma}_i - 1) = 0, &&& \text{for all } i = 1, \dots, n_T \\ 0 \leq \bar{w}_k \leq 1, &&& \text{for all } k = 1, \dots, n_s \\ 0 \leq \bar{\sigma}_i \leq 1, &&& \text{for all } i = 1, \dots, n_T. \end{aligned}$$

Proof. Notice that the state system of the optimal placement problem is a linear one, which has a unique solution thanks to Theorem 4. Therefore, the state system is a linear bijection and the adjoint system, which is the transpose operator of the state system, is also a linear bijection. Consequently, the adjoint system (26) also has a unique solution $(\eta_j, \zeta_j, \tau_j) \in L^2(Q) \times H^{2,1}(Q) \times H^1(\Omega)$, for all $j = 1, \dots, N$. Similarly as in the study of the data assimilation adjoint equation, the solution η_j to (26a) exhibits extra regularity. In fact, as the right-hand side of this equation belongs to $L^2(0, T; \mathcal{M}(\Omega))$, using Theorem 2 we get that $\eta_j \in L^2(0, T; W^{1,r}(\Omega))$, with $r \in [1, \frac{n}{n-1}]$.

To obtain the gradient system for the bilevel problem, we take the derivative of the reduced cost functional with respect to the decision variables $\mathbf{w} = (w, \sigma)$, in a direction $h = (h^1, h^2) \in \mathbb{R}^{n_s} \times \mathbb{R}^{n_T}$. Proceeding in a similar way as in the proof of Theorem 3 (see also [9, Chapter 3]), for the first n_s components, we get

$$\nabla_{w_k} F(\mathbf{w})(h_k^1) = \gamma_w h_k^1 - \sum_{j=1}^N \int_0^T \sum_i h_k^1 \sigma_i \rho_i(t) \zeta_j(x_k, t) (y_j(x_k, t) - z_{oj}(x_k, t)) dt$$

and, for the next n_T components,

$$\nabla_{\sigma_i} F(\mathbf{w})(h_i^2) = \gamma_\sigma h_i^2 - \sum_{j=1}^N \int_0^T \sum_k w_k h_i^2 \rho_i(t) \zeta_j(x_k, t) (y_j(x_k, t) - z_{oj}(x_k, t)) dt.$$

Consequently, the $n_s + n_T$ terms of the reduced cost gradient are given by

$$\begin{aligned} \nabla F(\mathbf{w})_k &= \gamma_w - \sum_{j=1}^N \int_0^T \sum_i \sigma_i \rho_i(t) \zeta_j(x_k, t) (y_j(x_k, t) - z_{oj}(x_k, t)) dt, \quad \forall k = 1, \dots, n_s, \\ \nabla F(\mathbf{w})_{n_s+i} &= \gamma_\sigma - \sum_{j=1}^N \int_0^T \sum_k w_k \rho_i(t) \zeta_j(x_k, t) (y_j(x_k, t) - z_{oj}(x_k, t)) dt, \quad \forall i = 1, \dots, n_T. \end{aligned}$$

Since the admissible $V_{ad} \subset \mathbb{R}^{n_s} \times \mathbb{R}^{n_T}$ is convex and closed, and the cost functional is differentiable, the necessary optimality condition is given through the variational inequality

$$(27) \quad \nabla F(\bar{\mathbf{w}})(v - \bar{\mathbf{w}}) \geq 0, \quad \forall v \in V_{ad},$$

where $\bar{\mathbf{w}} \in V_{ad}$ is the optimal solution of (21) (see [9, p.30]). Moreover, inequality (27) can also be expressed in terms of the projection onto V_{ad} as:

$$(28) \quad \bar{\mathbf{w}} = P_{V_{ad}}(\bar{\mathbf{w}} - c \nabla F(\bar{\mathbf{w}})), \quad \forall c > 0.$$

Defining the Karush-Kuhn-Tucker multipliers

$$\lambda^a = \max\{0, \nabla F(\bar{\mathbf{w}})\} \quad \text{and} \quad \lambda^b = |\min\{0, \nabla F(\bar{\mathbf{w}})\}|,$$

equation (28) can be rewritten as

$$\nabla F(\bar{\mathbf{w}}) - \lambda^a + \lambda^b = 0,$$

jointly with $\lambda^a(v - \bar{\mathbf{w}}) \geq 0$, $\lambda^b(v - \bar{\mathbf{w}}) \geq 0, \forall v \in V_{ad}$. $\lambda^a, \lambda^b \geq 0$, and $0 \leq \bar{\mathbf{w}} \leq 1$. In particular, taking v equal to the lower bound of V_{ad} in the first inequality and equal

to the upper one in the second case, we obtain the following complementarity system:

$$(29) \quad \begin{aligned} \lambda_\ell^a &\geq 0, \lambda_\ell^b \geq 0, & \forall \ell = 1, \dots, n_s + n_T \\ \lambda_k^a \bar{w}_k &= \lambda_k^b (\bar{w}_k - 1) = 0, & \forall k = 1, \dots, n_s \\ \lambda_{n_s+i}^a \bar{\sigma}_i &= \lambda_{n_s+i}^b (\bar{\sigma}_i - 1) = 0, & \forall i = 1, \dots, n_T \\ 0 &\leq \bar{w}_k \leq 1, & \forall k = 1, \dots, n_s \\ 0 &\leq \bar{\sigma}_i \leq 1, & \forall i = 1, \dots, n_T. \end{aligned}$$

□

3.4. Sparsity enforcing penalty function. Due to the kind of problem we deal with, the solutions that we would like to get are binary vectors that clearly establish the optimal sensors' location and when the devices should be turned on. Sparsity enforcing penalty functions enhance the sparsity on the solution vectors. In particular, we consider a modification of the objective functional in the following way:

$$\min_{0 \leq \mathbf{w} \leq 1} J(\mathbf{y}, \mathbf{w}) = \sum_{j=1}^N \|y_j^\dagger - y_j\|^2 + \beta \sum_{j=1}^N \|u_j^\dagger - u_j\|^2 + \gamma_w \Phi_\epsilon(w) + \gamma_\sigma \Phi_\epsilon(\sigma),$$

where $\Phi_\epsilon(\cdot)$ is a penalty function that enhance sparsity. In particular, we consider here the family of penalization functions proposed in [1, p.2135]:

$$\Phi_\epsilon(x) = \sum_i g_\epsilon(x_i) \text{ and } g_\epsilon(x_i) = \begin{cases} \frac{x_i}{\epsilon}, & 0 \leq x_i \leq \frac{1}{2}\epsilon \\ \pi_\epsilon(x_i), & \frac{1}{2}\epsilon < x_i \leq 2\epsilon \\ 1, & 2\epsilon < x_i \leq 1 \end{cases}$$

with $\pi_\epsilon(\cdot)$ a uniquely defined polynomial of third order that makes $g_\epsilon : [0, 1] \rightarrow [0, 1]$ continuously differentiable. Setting $\pi_\epsilon(x) = ax^3 + bx^2 + cx + e$, its coefficients can be obtained for each value of $\epsilon > 0$ by solving the following system:

$$(30) \quad \begin{pmatrix} \frac{\epsilon^3}{8} & \frac{\epsilon^2}{4} & \frac{\epsilon}{2} & 1 \\ 8\epsilon^3 & 4\epsilon^2 & 2\epsilon & 1 \\ \frac{3\epsilon^2}{4} & \epsilon & 1 & 0 \\ 12\epsilon^2 & 4\epsilon & 1 & 0 \end{pmatrix} \begin{pmatrix} a \\ b \\ c \\ e \end{pmatrix} = \begin{pmatrix} \frac{1}{2} \\ 1 \\ \frac{1}{\epsilon} \\ 0 \end{pmatrix}$$

Since we modified the objective function, the optimality system must be altered as well. However, the only change occurs in the computation of the gradient equation, which takes the following form:

$$(31a) \quad \nabla F(\mathbf{w})_k = \gamma_w g'_\epsilon(w_k) - \sum_{j=1}^N \int_0^T \sum_i \sigma_i \rho_i(t) \zeta_j(x_k, t) (y_j(x_k, t) - z_{oj}(x_k, t)) dt,$$

for all $k = 1, \dots, n_s$, and

$$(31b) \quad \nabla F(\mathbf{w})_{n_s+i} = \gamma_\sigma g'_\epsilon(\sigma_i) - \sum_{j=1}^N \int_0^T \sum_k w_k \rho_i(t) \zeta_j(x_k, t) (y_j(x_k, t) - z_{oj}(x_k, t)) dt,$$

for all $i = 1 \dots, n_T$. If we define $\lambda_a = \max\{0, \nabla F(\bar{\mathbf{w}})\}$ and $\lambda_b = |\min\{0, \nabla F(\bar{\mathbf{w}})\}|$, the new gradient equation (31) verifies $\nabla F(\bar{\mathbf{w}}) - \lambda_a + \lambda_b = 0$, jointly with the complementarity system given by (29).

However, since Φ_ϵ is a concave function, the solution to the bilevel problem may not be unique. To deal with this issue, we proceed as in [2], i.e., for fixed parameters

γ_w and γ_σ , we solve the problem without sparsity enforcing penalty term. Then, we take the solution vectors w and σ as the initialization vectors for the problem with the nonconvex term. In practice, once ϵ is sufficiently small, w and σ will approach the binary vectors.

4. NUMERICAL SOLUTION OF THE BILEVEL PLACEMENT PROBLEM

In this section we describe the algorithmic framework utilized for the construction of the proposed solution algorithm and, after presenting it, we address its main convergence properties in the case of the placement problem under consideration.

4.1. Projected quasi-Newton methods. In general, a projection method to solve the box-constrained problem

$$\min_{w \in C} f(w)$$

makes use of a descent direction of the unconstrained instance and, thereafter, projects the new iterate onto the closed convex set C defined by the bound constraints ([9], pp.75). Thus, the update of the iterate w_k is given by

$$w_{k+1} = P_C(w_k + \alpha_k d_k),$$

where P_C stands for the projection onto the closed and convex set C , d_k is a descent direction, and $\alpha_k \in (0, 1)$ a line search parameter. A modified Armijo rule is given by choosing the largest α_k such that

$$(32) \quad f(P_C(w_k + \alpha_k d_k)) - f(w_k) \leq -\frac{\hat{\gamma}}{\alpha_k} \|P_C(w_k + \alpha_k d_k) - w_k\|^2,$$

where $\hat{\gamma} \in (0, 1)$.

Using a descent direction provided by a second order method, i.e., $d_k = -H_k^{-1} \nabla f(w_k)$, where H_k stands for the Hessian matrix or an approximation to it, one is tempted to think that the iterate of the corresponding projected second order method would simply be given by

$$(33) \quad w_{k+1} = P_C(w_k - \alpha_k H_k^{-1} \nabla f(w_k)).$$

However, there are several counterexamples that show that using (33) may lead to wrong solutions (see [16], pp.98), because the information provided by the Hessian matrix is not enough to generate descent directions for the constrained problem.

Instead of using the full Hessian matrix, it is necessary to use a reduced version of it, based on the estimation of ϵ -active and active sets defined as:

$$A^\epsilon(w) = \{i : a_i \leq w_i \leq a_i + \epsilon \text{ or } b_i \geq w_i \geq b_i - \epsilon\}, \text{ and } A(w) = \{i : w_i = a_i \text{ or } w_i = b_i\}.$$

where a_i and b_i stand for the lower and upper bounds, respectively. Their complements, $I^\epsilon(w)$ and $I(w)$ are called the ϵ -inactive and inactive sets, respectively.

In a general way, if S represents an index set, then R_S will denote the matrix $R_S = (\delta_{ij})$ if $i \in S$ or $j \in S$, with $\delta_{ij} = 1$ if $i = j$ and $\delta_{ij} = 0$ otherwise. With these notations, the reduced Hessian matrix, at an iterate w_k , is defined as:

$$\begin{aligned} \tilde{R}(w_k, \epsilon_k, H_k) &= R_{A^{\epsilon_k}(w_k)} + R_{I^{\epsilon_k}(w_k)} H_k R_{I^{\epsilon_k}(w_k)} \\ &= \begin{cases} d_{ij}, & \text{if } i \in A^{\epsilon_k}(w_k) \text{ or } j \in A^{\epsilon_k}(w_k), \\ (H_k)_{ij}, & \text{otherwise.} \end{cases} \end{aligned}$$

Now, with the reduced matrix, the iteration of the projected method is given by

$$(34) \quad w_{k+1} = P_C(w_k - \alpha_k \tilde{R}(w_k, \epsilon_k, H_k)^{-1} \nabla f(w_k)).$$

If H_k corresponds to the exact Hessian matrix, (34) represents the iterations of the projected Newton method, which converges q-quadratically upon identification of the active set (see [16, Theorem 5.5.3]).

Let now H_k be an approximation of the Hessian matrix provided by the BFGS method. A possible update of the second term in the approximation $\tilde{R}(w_{k+1}, \epsilon_{k+1}, H_{k+1})$ is given by (see [16, p.102]):

$$\tilde{H}_{k+1} = R_{I^{\epsilon_k}(w_k)} H_k R_{I^{\epsilon_k}(w_k)} - R_{I^{\epsilon_k}(w_k)} \frac{H_k s_k s_k^T H_k}{s_k^T H_k s_k} R_{I^{\epsilon_k}(w_k)} + \frac{y_k^\# (y_k^\#)^T}{s_k^T y_k^\#},$$

where

$$(35) \quad y_k^\# = R_{I^{\epsilon_k}(w_k)} (\nabla f(w_{k+1}) - \nabla f(w_k)).$$

Similarly to the unconstrained case, there is also an update to the inverse matrix of the BFGS projected method $B_k = H_k^{-1}$, which is given by

$$(36) \quad \tilde{B}_{k+1} = \left(I - \frac{s_k^\# (y_k^\#)^T}{(y_k^\#)^T s_k^\#} \right) R_{I^{\epsilon_k}(w_k)} B_k R_{I^{\epsilon_k}(w_k)} \left(I - \frac{y_k^\# (s_k^\#)^T}{(y_k^\#)^T s_k^\#} \right) + \frac{s_k^\# (s_k^\#)^T}{(y_k^\#)^T s_k^\#},$$

where $s_k^\# = R_{I^{\epsilon_k}(w_k)}(w_{k+1} - w_k)$. The descent direction is then given by

$$(37) \quad d_k = -R_{A^{\epsilon_k}(w_k)} \nabla f(w_k) - \tilde{B}_k \nabla f(w_k).$$

4.2. Algorithm. We propose next a projected BFGS algorithm to solve the optimal observation placement problem (19). What we aim to obtain is an optimal placement vector $\mathbf{w} = (w, \sigma)$ that will enable to obtain the best average reconstruction of each training pair $(u_j^\dagger, y_j^\dagger)$.

The algorithmic procedure is as follows. After setting the parameter values, the first stage consists in solving the N data assimilation problems given by (18b), by means of a standard BFGS method. In the second stage, the solutions of the N corresponding adjoint systems for the bilevel problem are computed. Notice that these two stages of the algorithm can be computed in parallel, since for each $j = 1, \dots, N$ the systems are independent from each other. In the third stage, we compute the gradient of the bilevel problem, estimate the ϵ -active sets, and finally using the BFGS projected method, calculate the placement vector update.

Concerning the line search, we will require that the parameter α belongs to the following set

$$\left\{ \frac{1}{2^i \|\nabla F(\mathbf{w}_0)\|}, i \in \{0, 1, 2, \dots\} \right\},$$

where $\nabla F(\mathbf{w}_0)$ represents the gradient of the given initial placement vector \mathbf{w}_0 .

Intuitively, if the iterations of the projected BFGS start close to a non-degenerate local minimum hand with a good approximation of the Hessian, it is expected that the iterations of the method will converge q-superlinearly.

Theorem 7. *Let \bar{w} be a non-degenerate local minimizer. If w_0 is close enough to \bar{w} , $A(w_0) = A(\bar{w})$, and $R_{I^{\epsilon_0}(w_0)}$ is taken sufficiently near to $R_{I(\bar{w})} \nabla^2 f(\bar{w}) R_{I(\bar{w})}$ then the projected BFGS iterations converge q-superlinearly to \bar{w} .*

Proof. It is easy to see that the reduced cost functional F is twice differentiable and, due to the linear-quadratic nature of the problem, its Hessian does not depend on \mathbf{w} . Consequently, it is also globally Lipschitz continuous and all conditions of [16, Thm. 4.1.3.] are verified. \square

Algorithm 1

-
1. Set the values of $m, n, \mathbf{w}_0 = (w_0, \sigma_0), \alpha, \beta, \gamma, \gamma_\sigma$, and $k = 0$.
 2. Compute $\nabla F(\mathbf{w}_0)$.
 3. **Repeat**
 4. For each $j = 1, \dots, N$, find $(y_{k_j}, p_{k_j}, u_{k_j})$ solution of (19b).
 5. For each $j = 1, \dots, N$, find $(\eta_{k_j}, \zeta_{k_j})$ solution of (26).
 6. Find $\nabla F(\mathbf{w}_k)$ using (3.3).
 7. Estimate the ϵ -active set of (w_k, σ_k) .
 8. Compute \tilde{B}_{k+1} according to (36).
 9. Find a descent direction d_k using (37).
 10. Find $\alpha_k \in \left\{ \frac{1}{2^i \|\nabla F(\mathbf{w}_0)\|}, i \in \{0, 1, 2, \dots\} \right\}$ that verifies (32).
 11. Update $w_{k+1} = P_{V_{ad}}(\mathbf{w}_k + \alpha_k d_k)$
 12. Set $k = k + 1$.
 13. **Until** stopping criteria
-

5. COMPUTATIONAL EXPERIMENTS

In this section we report on the computational results obtained by using the algorithm described above. The spatial domain consists in the unit square $\Omega =]0, 1[\times]0, 1[$, while the used time interval is $[0, T] = [0, 14]$, divided in 14 possible time subintervals. For the discretization, we use finite differences in space and an implicit Euler method in time, with spatial and time discretization steps $h = 1/(m - 1)$ and $\tau = 1/(n + 1)$, respectively.

The study is divided in two sets of numerical experiments. In section 5.1, we provide a numerical study of our method considering just one element of the training set. Here, we will observe how the solution vectors vary when we use different penalization parameters. Furthermore, we will compare the results when different sparsity enforcing functions are implemented. Thereafter, in section 5.2, we use a larger training set and focus on learning the optimal placement vectors' structure. For all these experiments, we set $m = 10$, yielding $m^2 = 100$ possible points inside the unit square, where the location of a sensor is possible. The background error covariance information B^{-1} will be set as σI , where I is the identity operator and σ takes the value of 1×10^{-4} .

Due to the relaxation of the integer constraints in the formulation of the bilevel problem, w and σ may take values between zero and one. To better classify the entries of these vectors, we divide the constraint interval $[0, 1]$ into subintervals and count the number of elements of the vectors that belong to each one of them. For the placement vector w , we fix the following intervals: $\mathbf{I}_1 \mathbf{w} =]0, 0.005]$, $\mathbf{I}_2 \mathbf{w} =]0.005, 0.75]$ and $\mathbf{I}_3 \mathbf{w} =]0.75, 1[$. Moreover, $\mathbf{0w}$'s and $\mathbf{1w}$'s denote the number of null entries and ones of w . For the time subintervals placement vector σ , we consider the following subintervals: $\mathbf{I}_1 \mathbf{s} =]0, 0.25]$, $\mathbf{I}_2 \mathbf{s} =]0.25, 0.50]$, $\mathbf{I}_3 \mathbf{s} =]0.5, 0.75]$, and $\mathbf{I}_4 \mathbf{s} =]0.75, 1[$. Likewise, $\mathbf{0s}$'s and $\mathbf{1s}$'s denote the null entries and the ones of σ .

5.1. Single training pair experiments. In this first set of experiments, we will compute the training state y^\dagger by solving the variational data assimilation problem using $u^\dagger(x, y) = \sin(x) + y$. To illustrate the behavior of the lower level problem, for the given initial condition, we provide few snapshots of the model problem's evolution, see Figure 1.

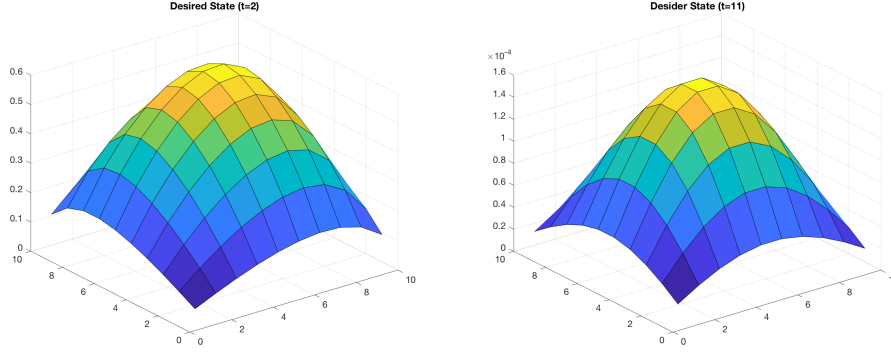


Figure 1. Snapshots of the state at times $t = 2$ (left) and $t = 11$ (right).

5.1.1. *Experiment 1.* The structure of the optimal placement vector, both in time and space, depends on the value of the penalization parameters γ_w , γ_σ , and β . The main objective in this experiment is to observe how $\mathbf{w} = (w, \sigma)$ changes when we work with different values of these parameters. We perform the experiments in two stages. In the first one, we fix the parameters γ_σ and β , and let γ be the one that changes. Here, γ_w represents the penalization parameter of the location vector w . In the second stage, we vary the values of γ_σ , while keeping the values of γ_w and β fix. γ_σ represents the penalization parameter of the time intervals vector σ . Hereafter, we will denote the cases when we work with a linear sparsity enforcing penalty function as *Case I*, and the ones when we include the concave sparsity enforcing function Φ_ϵ as *Case II*.

First setting: $\gamma_\sigma = 0.0001$ and $\beta = 0.01$. Table 1 contains the information about the number of entries of the vectors w and σ in each one of the fixed subintervals, and how they change depending on the parameters. As expected, when the penalization parameter increases, the decision vector becomes sparser. This, however, doesn't occur in a predictable way. Compare, for instance, the solution vectors for $\gamma_w = 0.003$ and $\gamma_w = 0.004$.

γ_w	0w's	I ₁ w	I ₂ w	I ₃ w	1w's	0s's	I ₁ s	I ₂ s	I ₃ s	I ₄ s	1s's
0.0001	0	0	0	1	99	0	0	0	0	0	14
0.001	0	0	0	8	92	0	0	0	0	0	14
0.002	0	0	0	13	87	0	0	0	0	0	14
0.003	20	0	0	0	80	0	0	0	0	0	14
0.004	0	28	0	1	71	0	0	0	0	0	14
0.005	34	0	1	0	65	0	0	0	0	0	14
0.006	40	0	2	0	58	0	0	0	0	0	14
0.007	46	0	0	0	54	0	0	0	0	0	14
0.008	53	0	0	0	47	0	0	0	0	0	14
0.009	56	0	2	42	0	0	0	0	0	14	0
0.01	63	0	0	37	0	0	0	0	0	14	0
0.02	100	0	0	0	0	0	0	0	0	14	0

Table 1. Experiment 1. Setting 1 - *Case I*. Changes in w 's structure with different values of γ_w

For every choice of the parameters, in each iteration of the algorithm, the cost functional value has to decrease. To verify this, we show in Table 2 the initial and the last value of the cost functional, denoted as \mathbf{J}_0 and \mathbf{J}_{end} , respectively, and in Figure

2 the behaviour of the cost functional value along the iterations, for three different values of γ_w . Moreover, we also present in Table 2, the number of iterations that the algorithm requires to reach the optimal vectors and the values of their norms, which are given by $\|w\| = \sum_k w_k$ and $\|\sigma\| = \sum_i \sigma_i$.

γ_w	\mathbf{J}_0	\mathbf{J}_{end}	iter	$\ w\ $	$\ \sigma\ $
0.0001	0.031631	0.031631	3	99.9998	14
0.001	0.12163	0.12163	3	99.9896	14
0.002	0.22163	0.22159	3	99.9642	14
0.003	0.32163	0.26179	6	80	14
0.004	0.42163	0.30984	6	71.972	14
0.005	0.52163	0.34856	6	65.2994	14
0.006	0.62163	0.37628	6	58.998	14
0.007	0.72163	0.40048	5	54	14
0.008	0.82163	0.39883	5	47	14
0.009	0.92163	0.38948	7	40.664	13.1598
0.01	1.0216	0.31017	6	28.5823	10.8149
0.02	2.0216	0.026631	5	0	14

Table 2. Experiment 1. Setting 1 - *Case I*. Decreasing of $\|w\|$ for different values of γ_w

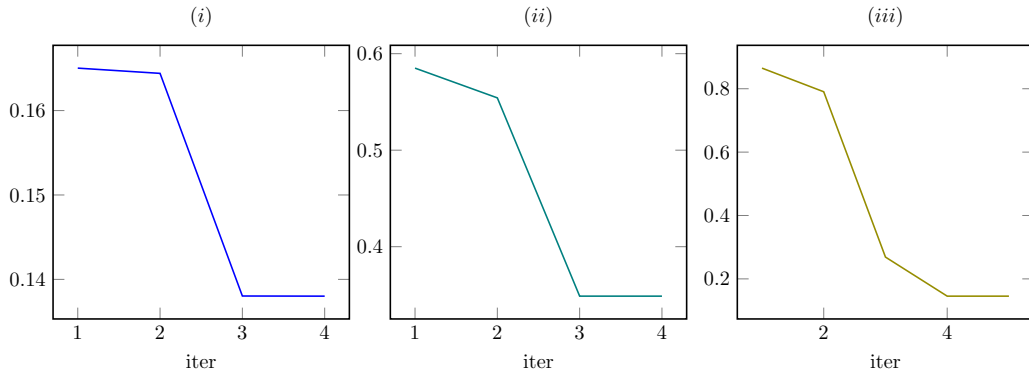


Figure 2. Decreasing of the objective function *Case I*. Different values of γ_w . (i) $\gamma_w = 0.002$, (ii) $\gamma_w = 0.007$, (iii) $\gamma_w = 0.01$.

The resulting structure of the optimal placement vector w can be visualized in Figure 3 for five different increasing values of γ_w . Apart of the increasing sparsity, the bilevel criterion favours the location of the observations in the upper-right corner of the domain, where the training initial condition actually plays a more relevant role.

In Table 3 we show the obtained results when the sparsity enforcing penalty function Φ_ϵ is used. As expected, utilizing Φ_ϵ forces w 's elements to be 0 or 1, which reduces the number of entries in between. Figure 4 shows this change graphically. In fact, comparing Figures 3 and 4 we can see that each component of w that was close to zero in the first case, reaches this value in the second one.

Second setting: $\gamma_w = 0.0001$ and $\beta = 0.001$. Now, by fixing the parameters γ_w and β and letting γ_σ be the one that varies, we obtain changes in the structure of time interval vector σ . These changes are reported in Table 4. As expected, as the penalization parameter increases, the structure of σ also becomes sparser.

In Table 5 we show the number of iterations that the algorithm requires to reach the solution. As in the previous realization, the norm of the time intervals vector decreases

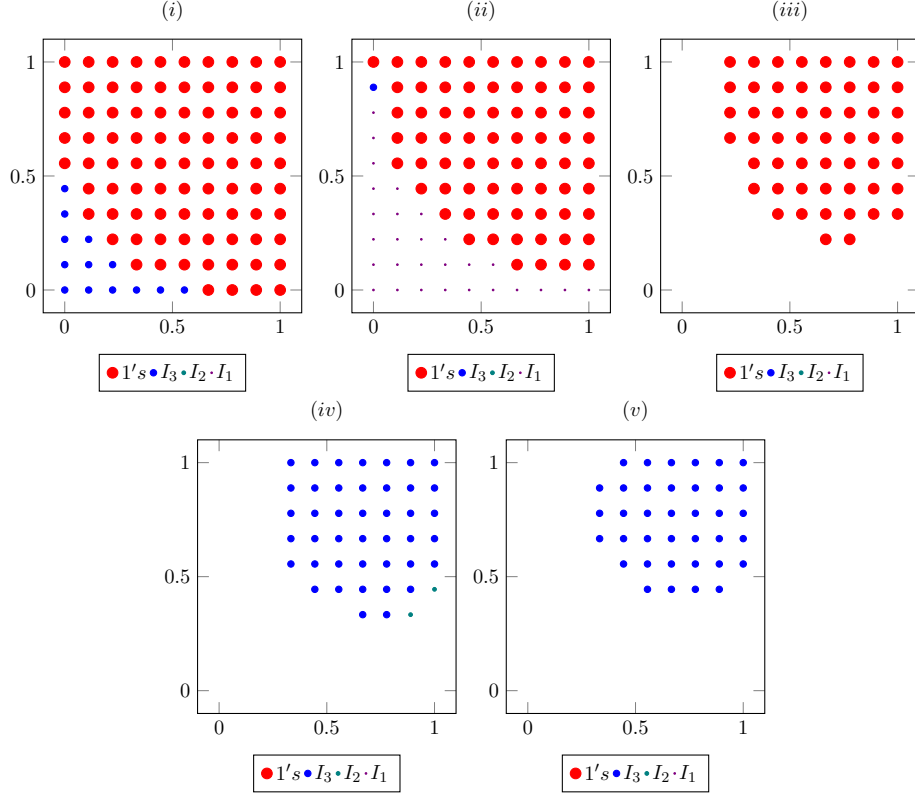


Figure 3. Optimal placement vector's structure *Case I*. Different values of γ . (i) $\gamma = 0.002$, (ii) $\gamma = 0.004$, (iii) $\gamma = 0.007$, (iv) $\gamma = 0.009$, (v) $\gamma = 0.01$.

ϵ	γ_w	$0w's$	I_1w	I_2w	I_3w	$1w's$
	0.0001	0	0	0	0	100
	0.001	0	0	0	0	100
	0.002	0	0	0	0	100
	0.003	20	0	0	0	80
	0.004	28	0	0	0	72
$\frac{1}{2}$	0.005	34	0	1	0	65
	0.006	40	0	1	1	58
	0.007	46	0	0	0	54
	0.008	6	47	0	0	47
	0.009	60	0	0	0	40
	0.01	90	0	3	6	1
	0.02	100	0	0	0	0

Table 3. Experiment 1. Setting 1 - *Case II*. Changes in w 's structure

as the penalization parameter increases. In Figure 5, we can observe the structure of the time intervals when the sensors/devices have to be turned on or turned off according to the choosing parameters.

It can be observed in Table 4 that, for almost every chosen value of γ_σ , the vector σ is already sparse. Therefore, the use of the sparsity penalization function Φ_ϵ does not bring significant changes.

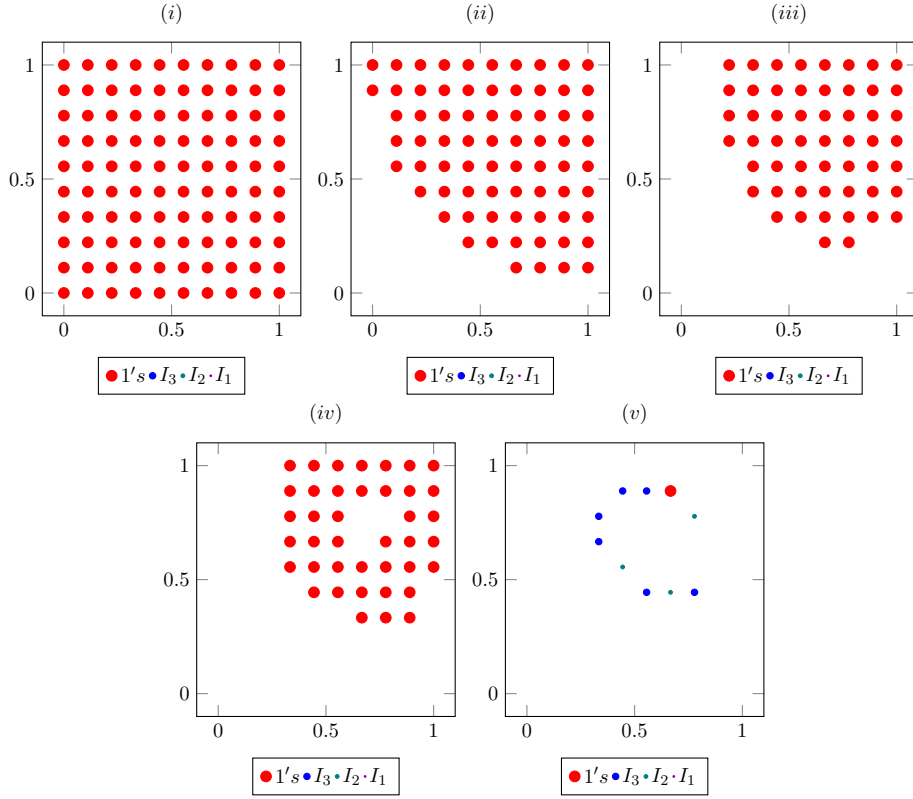


Figure 4. Optimal placement vector's structure *Case II*. Different values of γ_w . $(i)\gamma_w = 0.002$, $(ii)\gamma_w = 0.004$, $(iii)\gamma_w = 0.007$, $(iv)\gamma_w = 0.009$, $(v)\gamma_w = 0.01$.

γ_σ	0s's	I ₁ s	I ₂ s	I ₃ s	I ₄ s	1s's	0w's	I ₁ w	I ₂ w	I ₃ w	1w's
0.001	0	0	0	0	1	13	0	0	0	1	99
0.003	0	0	0	0	1	13	0	0	0	1	99
0.005	0	0	0	0	3	11	0	0	0	1	99
0.01	3	0	0	0	0	11	0	1	0	0	99
0.02	0	5	0	0	0	9	1	0	0	0	99
0.03	6	0	0	0	0	8	0	0	1	0	99
0.04	6	0	0	0	0	8	0	0	1	0	99
0.05	8	0	0	0	0	6	0	0	1	0	99
0.06	10	0	0	4	0	0	1	0	99	0	0
0.07	14	0	0	0	0	0	99	0	1	0	0

Table 4. Experiment 1. Setting 2 - *Case I*. Changes in σ 's structure with different values of γ_σ

5.1.2. *Experiment 2.* In many situations there are physical places where the location of a sensor results to be very difficult, i.e., not all points in the spatial domain are feasible. In order to get a more realistic experiment, we consider next just a small subset of locations as feasible placements. For this experiment, we take into account six specific spatial points of the domain. Considering that the given points do not have to correspond to the mesh nodes, we took the closer mesh point to each of them. The considered points are:

$$\begin{aligned}
 x_1 &= (0.1, 0.3) & x_2 &= (0.2, 0.2) & x_3 &= (0.5, 0.5) \\
 x_4 &= (0.7, 0.2) & x_5 &= (0.8, 0.8) & x_6 &= (0.6, 0.9)
 \end{aligned}$$

γ_σ	\mathbf{J}_0	\mathbf{J}_{end}	iter	$\ \mathbf{w}\ $	$\ \sigma\ $
0.001	0.039028	0.039026	3	99.9995	13.9947
0.003	0.067028	0.067003	3	99.9995	13.9829
0.005	0.095028	0.09495	3	99.9994	13.9682
0.01	0.16503	0.13801	5	99	11
0.02	0.30503	0.20862	5	99	9
0.03	0.44503	0.26874	5	99.3853	8
0.04	0.58503	0.34874	5	99.4978	8
0.05	0.72503	0.32877	5	99.6748	6
0.06	0.86503	0.14549	6	50.1596	2.0267
0.07	1.005	0.018876	6	0.71755	0

Table 5. Experiment 1. Setting 2 - *Case I*. Decreasing of $\|\sigma\|$ for different values of γ_σ

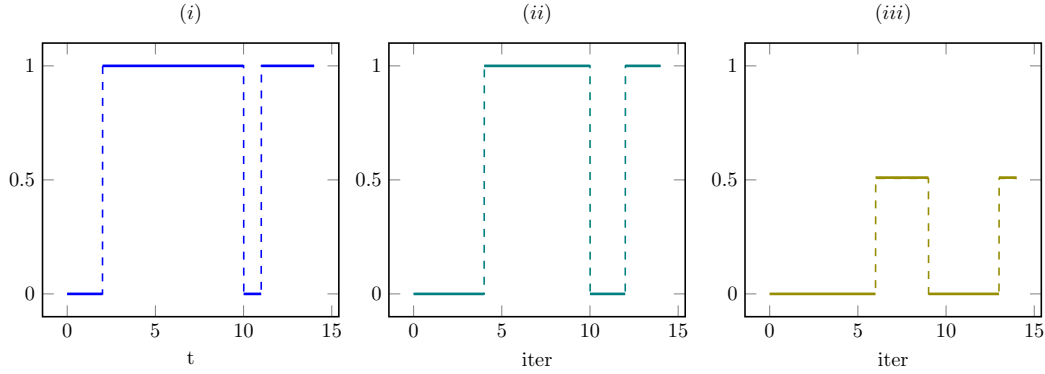


Figure 5. Optimal time intervals' structure *Case I*. Different values of γ_σ . (i) $\gamma_\sigma = 0.01$, (ii) $\gamma_\sigma = 0.04$, (iii) $\gamma_\sigma = 0.06$.

Similarly to the first experiment, we are interested in observing the changes in the structure of the placement vector w and the time intervals vector σ , for different values of the penalization parameters.

Table 6 shows the changes in the w structure when we fix $\gamma_\sigma = 0.01$ and $\beta = 0.1$, and let γ_w be the one that varies. Due to the small number of feasible points, the decrease of $\|w\|$ is not so aggressive in this case. We can verify this behavior in Table 7. Figure 6 shows graphically the location of these points, for different values of the penalization parameter.

γ_w	$0w$'s	I_1w	I_2w	I_3w	$1w$'s	$0s$'s	I_1s	I_2s	I_3s	I_4s	$1s$'s
0.01	0	0	0	0	6	0	0	0	0	13	1
0.03	0	0	0	2	4	0	0	0	0	13	1
0.06	0	0	0	3	3	0	0	0	0	13	1
0.09	0	0	0	4	2	0	0	0	0	13	1
0.1	0	0	0	5	1	0	0	0	0	13	1
0.2	0	0	0	6	0	0	0	0	0	13	1
0.3	6	0	0	0	0	14	0	0	0	0	0

Table 6. Experiment 2. *Case I*. Changes in w 's structure with different values of γ_w

γ_w	\mathbf{J}_0	\mathbf{J}_{end}	iter	$\ \mathbf{w}\ $	$\ \sigma\ $
0.01	0.28785	0.28657	4	6	13.8698
0.03	0.40785	0.40546	4	5.9636	13.8676
0.06	0.58785	0.5794	4	5.8808	13.8668
0.09	0.76785	0.74519	4	5.7621	13.8689
0.1	0.82785	0.79833	4	5.7171	13.8702
0.2	1.4279	1.2818	4	5.2739	13.8927
0.3	2.0279	0.089586	6	0	0

Table 7. Experiment 2. *Case I.* Decreasing of $\|\mathbf{w}\|$ for different values of γ_w

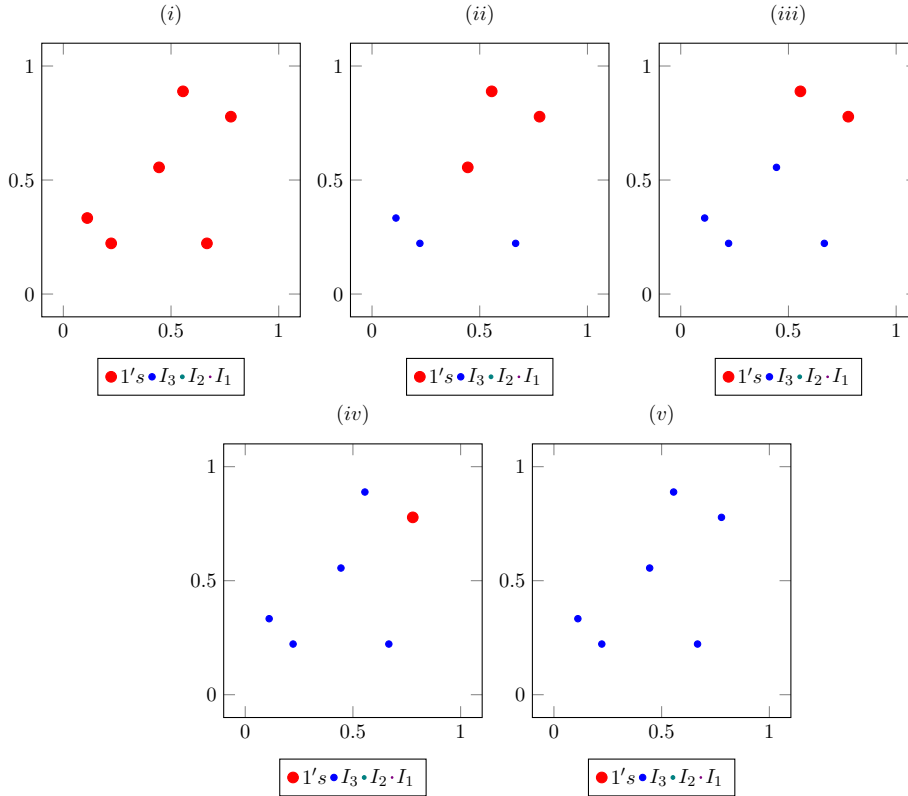


Figure 6. Optimal placement vector's structure *Case I.* Given points on the mesh. (i) $\gamma_w = 0.01$, (ii) $\gamma_w = 0.06$, (iii) $\gamma_w = 0.09$, (iv) $\gamma_w = 0.1$, (v) $\gamma_w = 0.2$.

5.2. Multiple training pairs. The second set of experiments considers a training set constituted by N pairs $(u_j^\dagger, y_j^\dagger)$, $j = 1, \dots, N$. As we mentioned before, the training set consists of improved reconstructions of the initial condition, with exceptionally more information. Given an enriched initial condition u^\dagger , y^\dagger is obtained through simulation of the system model. Therefore, to form the training set, we just have to fix $u_j^\dagger, j = 1, \dots, N$.

We start with a group of $N = 10$ different functions that, after a modification, will be our training initial conditions. The modification consists of summing a jump function to each one of the N functions. We consider this perturbation because a well-reconstructed initial condition must be able to capture discontinuities. For instance, in meteorology, the initial condition is affected by the topography of the region of

interest. The group of functions from which we will build the training set are:

$$\begin{aligned}
 u_1 &= \sin(x) + y, & u_4 &= \exp(\sin(xy)), & u_7 &= \sin(2\pi x) \sin(2\pi y) \\
 u_2 &= x^3 + xy - y, & u_5 &= \log(xy + 1), & u_8 &= \log(y \cos(x) + 1) \\
 u_3 &= \exp(y) + \cos(x), & u_6 &= \sin(x) \cos(y), & u_9 &= x^2 \cos(y + 1) \\
 & & & & u_{10} &= x^2 y^3 - 1.
 \end{aligned}$$

Figure 7 illustrates the modification carried out in the training initial conditions. It shows the form of the original u_2 and u_2^\dagger , respectively.

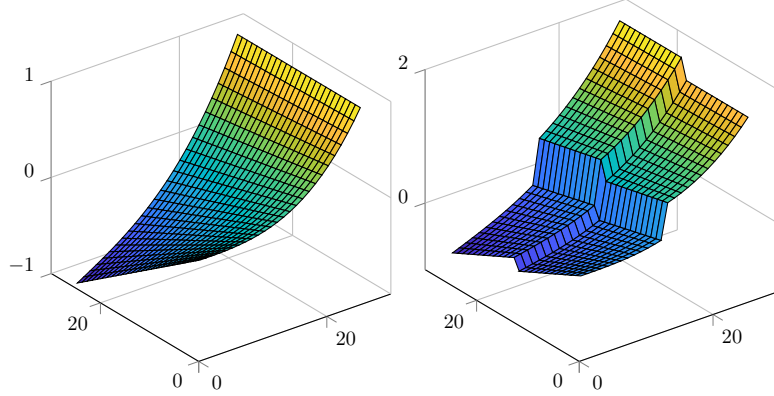


Figure 7. Modification of the training initial condition u_2^\dagger

5.2.1. *Experiment 3.* For this experiment, we vary the parameter γ_w of the placement vector, while $\gamma_\sigma = 1$ and $\beta = 1$ remain fix. In this case, the location vector $\mathbf{w} = (w, \sigma)$ has to be in average the optimal one for each training pair considered. Table 8 shows the structure of the resulting location vectors w and σ . As in the first experiment, the value of $\|w\|$ decreases as the penalization parameter increases. We can observe this behavior, as well as the number of iterations in Table 9, and the graphical representation of the location vector in Figure 8. In Figure 9 we also show the results when the sparsity enforcing penalty function Φ_ϵ is used.

γ_w	0w's	I ₁ w	I ₂ w	I ₃ w	1w's	0s's	I ₁ s	I ₂ s	I ₃ s	I ₄ s	1s's
1	0	0	0	0	100	0	0	0	0	0	14
3	0	0	0	7	93	0	0	0	0	0	14
5	0	0	1	18	81	0	0	0	0	0	14
6	0	0	6	17	77	0	0	0	0	0	14
7	0	0	7	25	68	0	0	0	0	0	14
9	0	0	10	35	55	0	0	0	0	0	14
15	0	0	28	37	35	0	0	0	0	0	14
19	1	0	33	38	28	0	0	0	0	0	14
35	1	5	47	30	17	0	0	0	0	0	14
40	14	0	46	40	0	0	0	0	0	14	0
50	40	0	40	15	5	0	0	0	14	0	0
65	70	0	22	6	2	0	0	14	0	0	0
85	90	0	10	0	0	0	14	0	0	0	0

Table 8. Experiment 3 - Case I. Changes in \mathbf{w} 's structure for different values of γ_w

γ_w	\mathbf{J}_0	\mathbf{J}_{end}	iter	$\ \mathbf{w}\ $	$\ \sigma\ $
1	126.2127	126.2127	3	100	14
3	326.2127	325.0621	15	99.5842	14
5	526.2127	515.5259	15	97.6503	14
6	626.2127	608.2746	15	96.7081	14
7	726.2127	698.1561	15	95.5834	14
9	926.2127	866.9141	15	92.7409	14
15	1526.2127	1288.2339	15	82.5247	14
19	1926.2127	1506.9064	15	76.9253	14
35	3526.2127	2338.9909	14	64.5235	14
40	4026.2127	2330.8975	15	56.1547	13.5671
50	5026.2127	1944.1406	15	35.5744	8.456
65	6526.2127	1197.7485	15	16.3581	5.124
85	8526.2127	294.1163	15	1.9015	2.662

Table 9. Experiment 3 - *Case I*. Decreasing of $\|\mathbf{w}\|$ for different values of γ_w

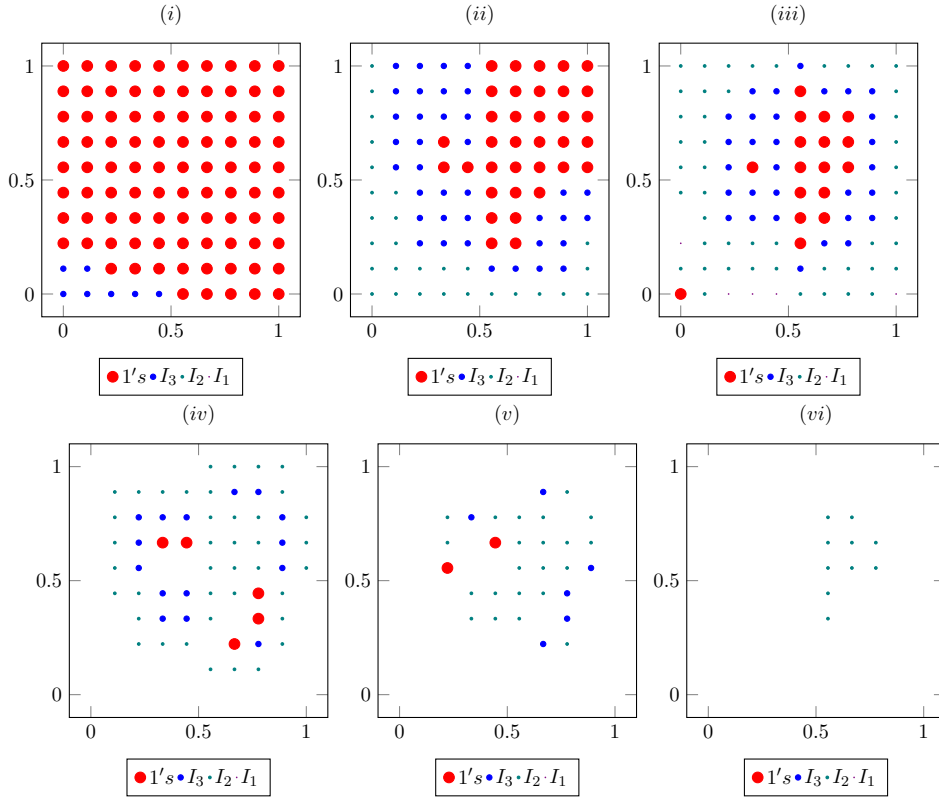


Figure 8. Optimal placement vector's structure. Different values of γ_w . (i) $\gamma_w = 3$, (ii) $\gamma_w = 15$, (iii) $\gamma_w = 35$, (iv) $\gamma_w = 50$, (v) $\gamma_w = 65$, (vi) $\gamma_w = 85$.

6. CONCLUSIONS

In this paper, we have proposed a bilevel learning approach for observation placement in variational data assimilation. The solution of our bilevel optimization problem

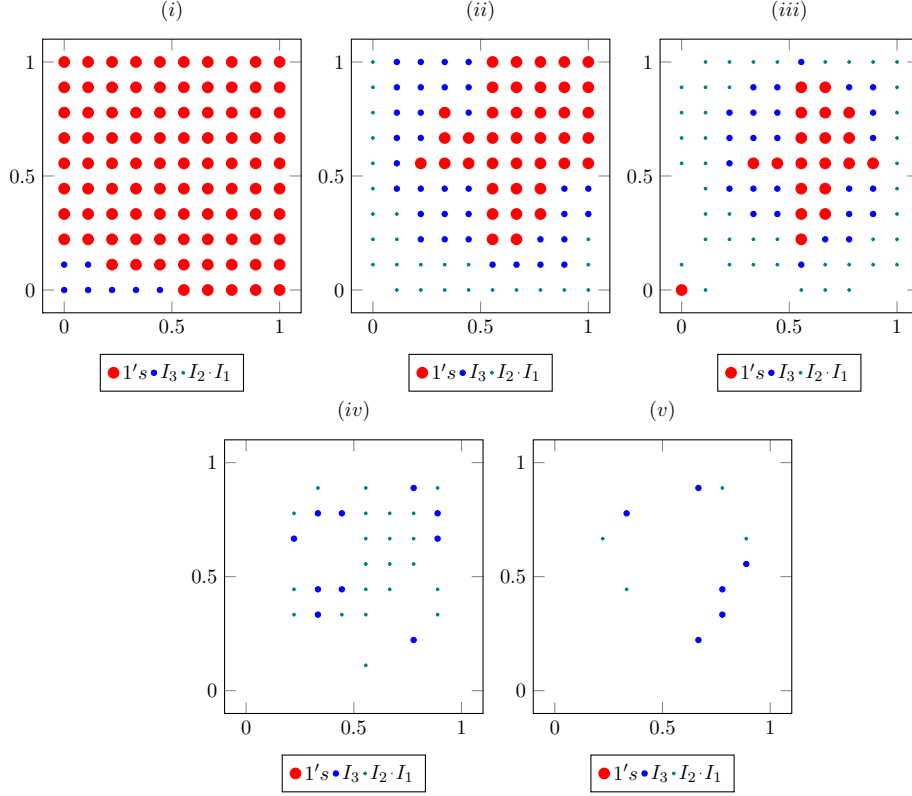


Figure 9. Optimal placement vector's structure *Case II*. (i) $\gamma_w = 3$, (ii) $\gamma_w = 15$, (iii) $\gamma_w = 35$, (iv) $\gamma_w = 50$, (v) $\gamma_w = 65$, (vi) $\gamma_w = 85$.

consists of two location vectors both in space and time. The first one provides the optimal configuration where the sensors/devices have to be placed, while the second one gives the optimal time subintervals at which the sensors have to be turned on.

We divided the study of the problem into two stages, the first one focused on the solution of the data assimilation problem which considered measures in space and mollified Dirac measures in time. We made a rigorous analysis of the function spaces where the solution belongs. Moreover, due to the presence of pointwise observations in the lower level cost functional, we have to deal with an adjoint system that has Borel measures on its right-hand side. We show the existence of a very weak solution of the adjoint state as well as useful estimations in terms of the solution vectors.

We used the optimality condition of the data assimilation problem as the constraint of the optimal location problem and considered a supervised learning approach in which we presuppose the existence of a training set of enriched reconstructed of initial conditions and their corresponding states. A first-order optimality system for the bilevel problem was then derived.

Numerically, both the lower and the upper problem were solved by using second-order methods. Specifically, the upper-level problem is solved by using a projected BFGS method where the approximation of the inverse of the reduced Hessian matrix is built iteratively by using the estimation of ϵ -active sets. We also show that the proposed projected algorithm preserves the superlinear convergence rate.

The performed experiments provide the structure of the locations vectors, showing that the solution becomes sparser as the penalization parameters increases. In some applications, one may wish to take into account economic factors and non-viable places

to locate sensors or devices. We considered these scenarios in some experiments to get more realistic results.

REFERENCES

- [1] A. Alexanderian, N. Petra, G. Stadler, and O. Ghattas. A-optimal design of experiments for infinite-dimensional bayesian linear inverse problems with regularized l_0 -sparsification. *SIAM Journal on Scientific Computing*, 36(5):A2122–A2148, 2014.
- [2] A. Alexanderian, N. Petra, G. Stadler, and O. Ghattas. A fast and scalable method for a-optimal design of experiments for infinite-dimensional bayesian nonlinear inverse problems. *SIAM Journal on Scientific Computing*, 38(1):A243–A272, 2016.
- [3] AV Balakrishnan and JL Lions. State estimation for infinite-dimensional systems. *Journal of Computer and System Sciences*, 1(4):391–403, 1967.
- [4] A. Bensoussan. *Filtrage Optimal des Systemes Lineaires*. Dunod, 1971.
- [5] John A Burns and Belinda B King. Optimal sensor location for robust control of distributed parameter systems. In *Decision and Control, 1994., Proceedings of the 33rd IEEE Conference on*, volume 4, pages 3967–3972. IEEE, 1994.
- [6] John A. Burns and Carlos N. Rautenberg. The infinite-dimensional optimal filtering problem with mobile and stationary sensor networks. *Numer. Funct. Anal. Optim.*, 36(2):181–224, 2015.
- [7] Eduardo Casas, Christian Clason, and Karl Kunisch. Parabolic control problems in measure spaces with sparse solutions. *SIAM Journal on Control and Optimization*, 51(1):28–63, 2013.
- [8] Ruth F. Curtain and Akira Ichikawa. Optimal location of sensors for filtering for distributed systems. pages 236–255. *Lecture Notes in Control and Informat. Sci.*, Vol. 1, 1978.
- [9] J.C. De los Reyes. *Numerical PDE-constrained optimization*. Springer, 2015.
- [10] Juan Carlos De los Reyes and Carola-Bibiane Schönlieb. Image denoising: Learning the noise model via nonsmooth PDE-constrained optimization. *Inverse Problems & Imaging*, 7(4), 2013.
- [11] E. Haber, L. Horesh, and L. Tenorio. Numerical methods for the design of large-scale nonlinear discrete ill-posed inverse problems. *Inverse Problems*, 26(2), 2010.
- [12] Roland Herzog and Ilka Riedel. Sequentially optimal sensor placement in thermoelastic models for real time applications. *Optim. Eng.*, 16(4):737–766, 2015.
- [13] Michael Hintermüller, Carlos N. Rautenberg, Masoumeh Mohammadi, and Martin Kanitsar. Optimal sensor placement: a robust approach. *SIAM J. Control Optim.*, 55(6):3609–3639, 2017.
- [14] Gernot Holler, Karl Kunisch, and Richard C Barnard. A bilevel approach for parameter learning in inverse problems. *Inverse Problems*, 34(11):115012, 2018.
- [15] Eugenia Kalnay. *Atmospheric modeling, data assimilation and predictability*. Cambridge university press, 2003.
- [16] C. Kelley. *Iterative methods for optimization*, volume 18. SIAM, 1999.
- [17] Olga Aleksandrovna Ladyzhenskaia, Vsevolod Alekseevich Solonnikov, and Nina N Ural'ceva. *Linear and quasi-linear equations of parabolic type*, volume 23. American Mathematical Soc., 1968.
- [18] J.L. Lions. *Optimal Control of Systems Governed by Partial Differential Equations*, volume 170. Springer Verlag, 1971.
- [19] Yannick Privat, Emmanuel Trélat, and Enrique Zuazua. Optimal shape and location of sensors for parabolic equations with random initial data. *Archive for Rational Mechanics and Analysis*, 216(3):921–981, 2015.
- [20] Friedrich Pukelsheim. *Optimal design of experiments*, volume 50 of *Classics in Applied Mathematics*. Society for Industrial and Applied Mathematics (SIAM), Philadelphia, PA, 2006.
- [21] F. Tröltzsch. Optimal control of partial differential equations. *Graduate studies in mathematics*, 112, 2010.

[†] RESEARCH CENTER ON MATHEMATICAL MODELING (MODEMAT), ESCUELA POLITÉCNICA NACIONAL, QUITO, ECUADOR.